RSC Advances

ROYAL SOCIETY OF CHEMISTRY

www.rsc.org/advances

PEDOT-PSS coated sulfur/carbon composite on porous carbon papers for high sulfur loading lithium-sulfur batteries

Zhijie Gong[a], Qixing Wu[b], Fang Wang[b], Xu Li[b], Xianping Fan, Hui Yang[a], Zhongkuan Luo[a,b*]

[a] Zhejiang California International NanoSystems Institute & Department of Materials Science and Engineering, Zhejiang University, 38 Zhe Da Road, Hangzhou, 310000, China

[b] College of Chemistry and Environmental Engineering, Shenzhen University, 3688 Nanhai Avenue, Nanshan District, Shenzhen, 518060 , China

*Corresponding author. E-mail address: lzk@szu.edu.cn; Tel: +86 755-26557249; Tax: +86 755-26557249.

Abstract: Increasing the sulfur loading in the cathode of a lithium-sulfur battery is an important way to improve its capacity for practical applications. To achieve this, the present work proposes using PEDOT-PSS to encapsulate sulfur/carbon black (S/BP) by a facile solution mixing method and the formed composite is then coated on a porous carbon paper. It is believed that the formation of core/shell structure in the PEDOT@S/BP composite can promote the electron transport and effectively impede the diffusion of polysulfides, and the porous carbon paper is able to retain the electrolyte containing the dissolved polysulfides in the cathode and alleviate the adverse effect of sulfur volumetric expansion. Due to such advantages, the proposed cathode, with a high sulfur loading of 3 mg cm^{-2}, can yield a high reversible capacity of 1041 mA h g^{-1} and an excellent cycle stability with a capacity retention of 868 mA h g^{-1} after 100 cycles and an average coulombic efficiency of 99.4%.

Keywords: Lithium–sulfur battery; cathode; PEDOT-PSS; sulfur-carbon composite; carbon paper

1. Introduction

Recently, conventional rechargeable lithium-ion batteries can hardly meet the requirements of high power energy systems, such as electric vehicles and high energy-consuming portable devices, due to its relatively low specific capacity. Therefore, explorations of advanced batteries with high energy densities are urgently needed. Among various batteries，lithium–sulfur (Li–S) battery is one of the most promising candidates, as it possesses a high theoretical specific capacity of 1672 mA h g^{-1} and energy density of 2600 W h kg^{-1}, which are three to five folds higher than those of the current lithium-ion batteries[1-4]. Moreover, as a cathode active material, sulfur has the advantages of low cost, light weight, and environmental benign[5]. However, Li-S batteries still face several challenges, including the insulating nature of sulfur (5×10^{-30} S cm^{-1}), the high solubility of lithium polysulfides as intermediate products into the electrolyte, and the large volume change (about 80%) during cycling. As a result, the Li-S battery generally suffers from a low utilization of the active material, a poor cycle life, and a low system efficiency, limiting its wide commercial applications[6].

In order to solve these aforementioned problems, various carbon materials, such as carbon black[7, 8], porous carbon[9-11], hollow carbon[12-14], carbon fiber[15, 16], carbon nanotube[17-19] and graphene/graphene oxide[20, 21] have been used as the supporting matrix for sulfur to improve conductivity of the cathode and prevent polysulfides dissolution. Among these materials, porous carbon with abundant micropores has been proved to be effective to improve the utilization of active materials and cycle stability of sulfur cathodes, due to its high conductivity, large surface area, and fine confinement of polysulfides[22, 23]. Guo et al.[24]

showed that a microporous carbon sphere with 37% micropores delivered a high reversible capacity of 600 mA h g^{-1} after 800 cycles at 1 C with a coulombic efficiency approaching 100% in each cycle. Chen et al. [25] reported a porous carbon microsphere with 46% micropores, which exhibited a superior rate performance and retained a high reversible capacity of 605 mA h g^{-1} at 2 C after 500 cycles. Li et al.[8] introduced the activated commercial conductive carbon black (Black Pearls 2000) as conductive substrate to support sulfur, which showed a high sulfur utilization of 1383.6 mA h g^{-1} after the initial activation. In addition, conductive polymers coatings have also been shown to be another effective way to provide good conductivity, buffer volume variations during cycling and trap polysulfides[26-28]. Gao et al.[29] synthesized a sulfur/carbon black composite coated with polyaniline by an in-situ polymerization method, and a high discharge capacity of 635.5 mA h g^{-1} at an ultrahigh rate (10 C) and 60% retention after 200 cycles were demonstrated. Cui et al.[30] systematically investigated a variety of conductive polymers and its coatings on sulfur, demonstrating poly(3,4-ethylenedioxythiophene) (PEDOT) was more suitable for surface coating to obtain a high specific capacity and long-term cycle life. Therefore, the preparation of conductive polymer/sulfur/microporous carbon multicomposites would be a promising way to improve the electrochemical performance of sulfur cathodes.

Although a large amount of high specific capacity and long-term cycle life cathodes for Li–S batteries have been reported in the literature, the sulfur loadings in the electrodes are generally lower than 2 mg cm^{-2}, which significantly reduces the overall energy density of cathode[21, 31, 32]. For a mass production of Li-S batteries, the sulfur cathodes requires a high sulfur loading (> 2 mg cm^{-2}) to obtain a higher areal capacity than those of state-of-the-art

lithium-ion batteries (2–4 mA h cm^{-2})[33]. This requirement of high sulfur loading can hardly be achieved with a traditional Al foil current collector, because a thick layer of active material tends to be peeled off after coating and drying[34] and prolongs the diffusion length of lithium ion so as to impose additional polarization and capacity loss[35]. In contrast, an interconnected porous current collector, such as graphene foam[34], carbon paper[36], self-waving carbon nanotubes[37], and carbon cloth[38], could be used to improve the energy density. The interconnected structure can not only support the active material with an intimate contact to achieve a higher sulfur loading (2-3 mg cm^{-2} or more), which is much higher than that on Al foils (usually less than 1 mg cm^{-2}), but also provide a remarkable absorption of electrolyte to minimize the ion transport resistance, thereby improving the electrochemical performance [39].

Herein, to increase the sulfur loading, we introduce the commercial conductive carbon black (BP) with abundant nanopores and high conductivity as the matrix to prepare S/BP composite by a melt infiltration process, and then the S/BP composite was coated with poly(3,4-ethylenedioxythiophene)-poly(styrene sulfonate) (PEDOT-PSS) via a simple solution mixing method. The formation of core/shell structure in the PEDOT@S/BP composite can promote the electron transport and effectively impede the diffusion of polysulfides. The as-prepared S/BP covered with PEDOT-PSS (PEDOT@S/BP) was then coated on a commercial porous carbon paper with an excellent conductivity and high porosity for the purpose of decreasing the cathode resistance, accommodating the active materials and retaining the electrolyte containing the dissolved polysulfides. Subsequently, the physical and electrochemical characteristics of the proposed PEDOT@S/BP cathode were evaluated experimentally and a comparative study between the PEDOT@S/BP and S/BP was also

presented and discussed.

2. Experimental

2.1 Preparation of the sulfur/carbon composite

The sulfur/carbon composite (S/BP) was prepared by the melt-diffusion process. The carbon black BP (Black Pearls 2000, Cabot Corporation) and sublimed sulfur (purity > 99.5%, Aladdin) with a weight ratio of 2:3 were milled by hand for 1 h. The mixture was then sealed in a glass vessel filled with argon gas, and heated at 155 ℃ for 20 h. At this temperature, the viscosity of melt sulfur is the lowest, which is in favor of the migration of sulfur into the pores of BP.

2.2 Preparation of the PEDOT-PSS coated S/BP composite

The PEDOT-PSS coated S/BP composite (PEDOT@S/BP) was synthesized via a solution mixing method. The fabrication procedures are illustrated in Fig 1. Typically, 0.5 g S/BP composite and 5 ml PEDOT-PSS solution (1 wt % in H_2O, Aldrich) were added into 95 mL deionized water with violent stirring for 12 h. Then the precipitate was collected by filtration and washed several times with deionized water and alcohol. Finally, the PEDOT@S/BP was obtained after drying at 60 ℃ for 24 h in a vacuum oven.

2.3 Materials characterizations

The morphologies of samples were examined using scanning electron microscopy (SEM Hitachi S-3400N II), field emission scanning electron microscopy (FESEM, Hitachi SU-70) and transmission electron microscopy (TEM, Tecnai G^2 Spirit120kv). The structural components of samples were characterized by X-ray diffraction (XRD, D8 Advance, Bruker) using Cu Kα radiation. The sulfur content was detected by using a TGA/DSC (STA409PC)

analyzer under heating at a rate of 10 °C min^{-1} in N_2 atmosphere. Nitrogen adsorption/desorption isotherm was measured with a nitrogen sorption instrument (BELL V-Sorb 2800TP) at 77 K. The specific surface area and the pore size distribution were calculated by the BET and BJH/HK methods.

2.4 Electrochemical characterizations

The 80 wt% S/BP or PEDOT@S/BP, 10 wt% acetylene black and 10 wt% binder (LA133) were mixed using deionized water–isopropanol as the solvent and stirred for 12 h to obtain homogeneous slurries. Working electrodes were prepared by coating the slurry onto Al foil and porous carbon paper current collectors (Toray carbon paper H-060) and drying at 40 °C for 24 h in a vacuum oven. Then, the S/BP coated on Al foil cathode (denoted as S/BP-Al hereafter), the S/BP coated on carbon paper cathode (denoted as S/BP-C hereafter) and the PEDOT@S/BP coated on carbon paper cathode were obtained. The sulfur loading was approximately 3 mg cm^{-2} on a carbon paper and 2 mg cm^{-2} on an Al foil. The specific capacity was calculated based on the sulfur mass. The electrolyte consisted of 1 M bis-(tri-fluoromethane) sulfonimide lithium (LiTFSI) in 1,2-dimethoxyethane (DME) and 1,3-dioxolane (DOL) (1 : 1, v/v) mixed solution with 1 wt % $LiNO_3$ as an additive. Lithium metal and Celgard 2400 membrane were used as the anode and separator, respectively. The CR2032 coin-type cells were assembled in a glove box filled with argon. The galvanostatic charge-discharge measurements were performed at ambient temperature by using the LAND CT2001A battery testing system in the potential range from 1.7 to 2.8 V (vs. Li/Li+). The cyclic voltammetries (CV) were carried out from 1.5 to 3.0 V at a scan rate of 0.1 mV s^{-1} by a CHI 660D electrochemical workstation. Measurements of electrochemical impedance spectra

(EIS) were conducted with an amplitude of 5 mV from 0.01 to 10^5 Hz at the condition of open circuit.

3. Results and Discussion

The nitrogen adsorption/desorption isotherms of BP in Fig. 2a exhibits a mixed type I and type II isotherms for low relative pressure (P/P_0) and high P/P_0[40, 41]. BP shows a strong nitrogen adsorption below the low relative pressure ($P/P_0 < 0.1$), indicating the existence of micropores on the surface of carbon particles [41]. Due to the gentle adsorption slope at P/P_0 = 0.1–0.9, the amount of mesopores is limited [42]. The sharp rise of adsorption curve after $P/P_0 >$ 0.9 represents the large porosity of BP contributed by the interspaces between the carbon particles, which can provide abundant channels for electrolyte. The BET surface area of BP is 1330 m^2 g^{-1} with a total pore volume of 3.0227 cm^3 g^{-1}. Fig. 2b exhibits the broad pore size distributions of BP ranging from 1.2–100 nm and the inset displays a large amount of micropores in BP. These results indicate that BP has a hierarchically porous structure with abundant micropores, which can confine polysulfides effectively and offer a close contact with the electrolyte.

The morphologies of BP, S/BP and PEDOT@S/BP are characterized by FESEM. It can be seen from Fig. 3a, BP exhibits a morphology of loose particles aggregated by small carbon spheres with a size of about 20-40 nm in diameter. After sulfur melted into carbon matrix, there is no apparent difference in morphology and size for S/BP composites (Fig. 3b). Thus, elemental sulfur diffuses, absorbs, and disperses in the host BP matrix by capillary force during the heating process. As show in Fig. 3c, it is obvious that the average size of PEDOT@S/BP particles is much bigger than S/BP particles, which is ascribed to the covering

of PEDOT-PSS. To further identify the microstructure of PEDOT@S/BP, the morphologies of S/BP and PEDOT@S/BP were investigated using TEM. In Fig. 3d, S/BP shows a chain-like structure without sulfur blocks in the matrix, which can provide a high conductivity. As compared with S/BP, PEDOT@S/BP appears a thin layer at the edge of the composite due to the addition of the PEDOT-PSS (see Fig. 3e), which indicates the PEDOT-PSS is indeed coated on the surface of S/BP composite. As shown in Fig. 3f, the thickness of PEDOT coating layer is 20-50 nm.

The XRD patterns of PEDOT-PSS, BP, sulfur, S/BP and PEDOT@S/BP are presented in Fig. 4. It can be observed that there are no sharp crystalline peaks in the XRD pattern of BP and PEDOT-PSS, indicating their amorphous structures. In contrast, the XRD pattern of sulfur exhibits several sharp peaks, suggesting its good crystal structure. After heat treatment, the characteristic peaks of the crystalline sulfur become weaker, which indicates that sulfur has diffused into the pores of BP. For PEDOT@S/BP, due to the introduction of the PEDOT-PSS, all characteristic peaks of crystal sulfur almost disappear, suggesting that the PEDOT-PSS layer is well coated on the surface of S/BP.

To determine the sulfur contents in the composites, the TG curves obtained in N_2 are shown in Fig. 5. The weight loss of pure sulfur is observed from 200 °C to 300 °C due to the evaporation of sulfur. Compared with the curves of pure sulfur, it is noted that the temperature for complete evaporation of sulfur in S/BP is up to 450 °C, indicating the strong adsorption of micropores of the BP matrix[8]. The sulfur content is 60% in S/BP calculated from the TG curves. For PEDOT@S/BP, the sulfur evaporation rate at the temperature range of 200–500 °C is much lower than that of S/BP, suggesting that the PEDOT-PSS layer

provides a strong confinement effect to improve the stability of sulfur. Due to the addition of PEDOT-PSS, the sulfur content in PEDOT@S/BP decreases to 56 %.

In order to evaluate the electrochemical performances of PEDOT@S/BP cathode, a series of electrochemical tests were conducted and the performances of S/BP-Al cathode and S/BP-C cathode were also presented for comparison. Cyclic voltammetry curves are shown in Fig. 6. For S/BP-Al cathode, two typical reduction peaks at about 2.3 V and 2.0 V appear during the first cycle corresponding to the two discharge plateaus in Fig. 5a, which are attributed to the conversion of elemental sulfur to soluble high-order lithium polysulfides (Li_2S_n, $4 \leq n < 8$) and the strong reduction of soluble polysulfide anions to insoluble low-order Li_2S_2 and Li_2S[2, 43, 44]. During the anodic scanning process, only one sharp oxidation peak is observed at the potential of approximately 2.4 V, which is associated with the interlaced conversions from lithium sulfides to low-order lithium polysulfides, high-order lithium polysulfides and sulfur. However, for S/BP-C cathode, three cathodic peaks are observed in the CV curve. The first and third reduction peaks at 2.2 V and 1.8 V, respectively, correspond to the same reduction reactions of S/BP-Al cathode. And the second reduction peak at 2.0 V shows the existence of poorly stable intermediate species which deeply depends on the first reduction process [45]. Meanwhile, the anodic peaks at 2.4 V and 2.5V are observed, which are assigned to the formation of the low-order lithium polysulfides and the high-order lithium polysulfides/sulfur[46]. Moreover, the current intensity of the anodic peaks on carbon paper is much higher than that on Al foil. All the above-mentioned comparisons demonstrate that the strong absorption of electrolyte by the porous carbon paper can facilitate the redox process. In addition, it is found that the CV features of PEDOT@S/BP cathode are similar to

those of S/BP-C cathode, except that the reduction peaks of PEDOT@S/BP cathode shift toward a higher potential and the oxidation potentials move to a lower potential. The shifts of potential indicate that the conductive PEDOT-PSS layer coated on the S/BP composite can effectively reduce the polarization and thus improves the electrochemical performance.

The charge-discharge profiles of S/BP-Al, S/BP-C and PEDOT@S/BP cathodes for the first cycle at 0.2 C are presented in Fig. 7a. The discharge curve of S/BP-Al cathode displays a typical two-plateau progress whereas the cathodes based on carbon papers exhibit three plateaus in the discharge curves, consistent with the CV curves. The small plateau (arrow) could be associated with the formation of S_4^{2-} and S_3^{2-} [45-47]. In addition, both of the discharge capacity and discharge voltage plateau of PEDOT@S/BP cathode are higher than those of S/BP-Al and S/BP-C cathodes, indicating more utilization of the sulfur and lower polarization of PEDOT@S/BP cathode. The rate capabilities of S/BP-Al, S/BP-C and PEDOT@S/BP cathodes at different rates from 0.2 C to 2 C are shown in Fig. 7b. All cathodes experience a sharp fall in capacity at 0.2 C. When the current density rises from 0.2 C to 2 C, the capacities of these cathodes decrease gradually. The PEDOT@S/BP cathode delivers a high initial discharge capacity of 1258, 805, 719, and 541 mA h g^{-1} at 0.2, 0.5, 1 and 2 C, respectively. When the current density is recovered to 0.2 C again, the capacity recover to 875 mA h g^{-1}. These results reveal the excellent rate performance of PEDOT@S/BP cathode at various rates. In contrast, S/BP-C cathode exhibits a lower discharge capacity and a faster capacity fading, indicating that the surface coating with PEDOT-PSS can promote the electron transport and effectively impede the diffusion of polysulfides. In the case of S/BP-Al cathode, the capacity is the lowest for all current

densities, demonstrating the importance of carbon papers for a high sulfur loading cathode.

The cycling performances of S/BP-Al, S/BP-C and PEDOT@S/BP cathodes are also evaluated at 0.2 C, as shown in Fig. 7c. All cathodes show a large decay in capacity at the second cycle, because of the dissolution of lithium polysulfides into the electrolyte[48]. Afterwards, the cycling performance of the batteries become relatively stable and hence the reversible capacities are calculated from the second cycle. For S/BP-Al cathode, the discharge capacity at the second cycle is 820 mA h g^{-1}. After 100 cycles, A capacity of 465 mA h g^{-1} is retained (only 56.7 % retention) with an average coulombic efficiency of 98.4 %, and the capacity decay is 0.432 % per cycle, whereas S/BP-C cathode delivers a high capacity of 920 mA h g^{-1}, retaining 667 mA h g^{-1} after 100 cycles with an average coulombic efficiency of 98.7 %, corresponding to a capacity retention of 72.5 %, and the capacity decay decreases considerably to 0.275 % per cycle. The improved cycling stability of S/BP-C cathode is attributed to the application of porous carbon papers, which can stabilize the active materials and reactions within the cathode region to facilitate the sulfur utilization[36]. As compared to the cathode with S/BP-C, the cathode with PEDOT@S/BP exhibits a higher discharge capacity of 1041 mA h g^{-1} at the second cycle. A reversible capacity of 868 mA h g^{-1} is obtained after 100 cycles. The capacity retention is as high as 83.4% and the capacity decay is only 0.166% per cycle, which are somewhat comparable to those in the similar reported literatures[6, 28]. Note that the sulfur loading in the cathode is 3 mg cm^{-2}, which is three times than those in the mentioned literatures. However, a high sulfur loading will not only thicken the cathode and thus increases the transport length of Li^+ and electron, but also aggravate the effect of volume expansion and contraction, accelerating the structural degradation of the

sulfur cathode[29, 34].

In order to evaluate the effect of various cathodes on the transport of polysulfides，we use the following formula to estimate the shuttle effect. According to the literature[49], the coulombic efficiency, C, can be related to the shuttle effect factor, *f*, by

$$C = \frac{2+(\ln(1+f))/f}{2-(\ln(1-f))/f} \quad (1)$$

Noted that the higher the shuttle effect factor, the severer the shuttle effect. As the average coulombic efficiencies of PEDOT@S/BP cathode and S/BP-C cathode for 100 cycles are 99.4% and 98.7%, respectively, the shuttle effect factors of these cathodes are 0.018 and 0.039 according to Eq.(1), which suggests that the PEDOT-PSS coating can more effectively inhibit the shuttle effect of polysulfides. To further characterize the electrochemical performances of S/BP-Al, S/BP-C and PEDOT@S/BP cathodes, the EIS tests are conducted. As presented in Fig. 7d, the S/BP-C cathode has a much smaller charge-transfer resistance Rct (51 Ω) than that of S/BP-Al cathode (110 Ω), which is attributed to the close contact between the activate materials and current collector. As compared with the S/BP-C cathode, the Rct of PEDOT@S/BP cathode further decreases to 35 Ω due to the increase in the electrical conductivity rendered by PEDOT.

The morphologies of S/BP-Al, S/BP-C and PEDOT@S/BP cathodes before and after 100 cycles at 0.2 C are shown in Fig. 8. Before cycling, some large cracks (~ 12 μm) are observed on the surface of S/BP-Al cathode while the cracks presented in the S/BP-C and PEDOT@S/BP cathodes are only ~ 1 μm. After 100 cycles, a number of cracks have appeared on the surface of S/BP-Al cathode, indicating the destruction of the electrode caused by the volume expansion during cycling. By contrast, the morphologies of carbon paper

cathodes only undergo little changes. Moreover, as can be seen from the cross-sectional images of carbon paper cathodes, numerous particles infiltrate into the interior of the carbon paper, which suggests that the porous carbon current collector can release stress to alleviate the volume expansion for high sulfur loading cathodes during the cycling process.

4. Conclusion

A high sulfur loading PEDOT@S/BP composite on a porous carbon paper has been prepared as the cathode of a Li-S battery via a facile method. The microporous structure of BP can provide an intimate contact and strong absorption of sulfur. The PEDOT-PSS layer plays an important role to promote the electron transportation and effectively impede the diffusion of polysulfides. Moreover, the carbon paper as the current collector can stabilize the active materials and reaction within the cathode region and remarkably alleviate the adverse effect of volume expansion by its unique physical properties. Therefore, the PEDOT@S/BP cathode with a high sulfur loading of 3 mg cm^{-2} delivers a high reversible specific capacity of 1041 mA h g^{-1} and a good capacity retention of 83.4% after 100 cycles at 0.2 C. In addition, the preparation of PEDOT@S/BP cathode is a facile and cost-effective method, which can advance the commercial applications of Li–S batteries.

Acknowledgements

This work was supported by Shenzhen Key Laboratory of New Lithium-Ion Battery and Mesoporous Materials, and Shenzhen Science and Technology Fund (No. JCYJ20130329102936684, No. JCYJ20140828163634002 and No. KQCX20140519105122378).

References

1. S. Evers and L. F. Nazar, *Accounts of chemical research*, 2012, 46, 1135-1143.
2. S. S. Zhang, *Journal of Power Sources*, 2013, 231, 153-162.
3. Y. Son, J.-S. Lee, Y. Son, J.-H. Jang and J. Cho, *Advanced Energy Materials*, 2015, 5.
4. A. Manthiram, Y. Fu, S.-H. Chung, C. Zu and Y.-S. Su, *Chemical reviews*, 2014, 114, 11751-11787.
5. D. Marmorstein, T. Yu, K. Striebel, F. McLarnon, J. Hou and E. Cairns, *Journal of Power Sources*, 2000, 89, 219-226.
6. H. Li, M. Sun, T. Zhang, Y. Fang and G. Wang, *Journal of Materials Chemistry A*, 2014, 2, 18345-18352.
7. Y.-J. Choi, Y.-D. Chung, C.-Y. Baek, K.-W. Kim, H.-J. Ahn and J.-H. Ahn, *Journal of Power Sources*, 2008, 184, 548-552.
8. G. Li, J. Hu, G. Li, S. Ye and X. Gao, *Journal of Power Sources*, 2013, 240, 598-605.
9. C. Liang, N. J. Dudney and J. Y. Howe, *Chemistry of Materials*, 2009, 21, 4724-4730.
10. W. Wang, X. Wang, L. Tian, Y. Wang and S. Ye, *Journal of Materials Chemistry A*, 2014, 2, 4316-4323.
11. J. Wang, J. Yang, J. Xie, N. Xu and Y. Li, *Electrochemistry Communications*, 2002, 4, 499-502.
12. S. Chen, X. Huang, H. Liu, B. Sun, W. Yeoh, K. Li, J. Zhang and G. Wang, *Advanced Energy Materials*, 2014, 4.
13. J. Kim, D. J. Lee, H. G. Jung, Y. K. Sun, J. Hassoun and B. Scrosati, *Advanced Functional Materials*, 2013, 23, 1076-1080.
14. N. Jayaprakash, J. Shen, S. S. Moganty, A. Corona and L. A. Archer, *Angewandte Chemie*, 2011, 123, 6026-6030.
15. R. Elazari, G. Salitra, A. Garsuch, A. Panchenko and D. Aurbach, *Advanced Materials*, 2011, 23, 5641-5644.
16. K. Fu, Y. Li, M. Dirican, C. Chen, Y. Lu, J. Zhu, Y. Li, L. Cao, P. D. Bradford and X. Zhang, *Chemical Communications*, 2014, 50, 10277-10280.
17. W. Ahn, K.-B. Kim, K.-N. Jung, K.-H. Shin and C.-S. Jin, *Journal of Power Sources*, 2012, 202, 394-399.
18. C.-P. Yang, Y.-X. Yin, Y.-G. Guo and L.-J. Wan, *Journal of the American Chemical Society*, 2015, 137, 2215-2218.
19. X. Z. Ma, B. Jin, P. M. Xin and H. H. Wang, *Applied Surface Science*, 2014, 307, 346-350.
20. N. Li, M. Zheng, H. Lu, Z. Hu, C. Shen, X. Chang, G. Ji, J. Cao and Y. Shi, *Chemical Communications*, 2012, 48, 4106-4108.
21. H. Wang, Y. Yang, Y. Liang, J. T. Robinson, Y. Li, A. Jackson, Y. Cui and H. Dai, *Nano letters*, 2011, 11, 2644-2647.
22. B. Zhang, X. Qin, G. Li and X. Gao, *Energy & Environmental Science*, 2010, 3, 1531-1537.
23. S. Xin, L. Gu, N.-H. Zhao, Y.-X. Yin, L.-J. Zhou, Y.-G. Guo and L.-J. Wan, *Journal of the American Chemical Society*, 2012, 134, 18510-18513.
24. H. Ye, Y.-X. Yin, S. Xin and Y.-G. Guo, *Journal of Materials Chemistry A*, 2013, 1, 6602-6608.
25. H. Xu, Y. Deng, Z. Zhao, H. Xu, X. Qin and G. Chen, *Chemical Communications*, 2014, 50, 10468-10470.
26. G. Ma, Z. Wen, J. Jin, M. Wu, X. Wu and J. Zhang, *Journal of Power Sources*, 2014, 267, 542-546.
27. L. Xiao, Y. Cao, J. Xiao, B. Schwenzer, M. H. Engelhard, L. V. Saraf, Z. Nie, G. J. Exarhos and J. Liu, *Advanced Materials*, 2012, 24, 1176-1181.
28. Y. Yang, G. Yu, J. J. Cha, H. Wu, M. Vosgueritchian, Y. Yao, Z. Bao and Y. Cui, *Acs Nano*, 2011, 5, 9187-9193.
29. G. C. Li, G. R. Li, S. H. Ye and X. P. Gao, *Advanced Energy Materials*, 2012, 2, 1238-1245.

30. W. Li, Q. Zhang, G. Zheng, Z. W. Seh, H. Yao and Y. Cui, *Nano letters*, 2013, 13, 5534-5540.
31. S. Evers, *Chemical Communications*, 2012, 48, 1233-1235.
32. Z. W. Seh, W. Li, J. J. Cha, G. Zheng, Y. Yang, M. T. McDowell, P.-C. Hsu and Y. Cui, *Nature communications*, 2013, 4, 1331.
33. S. S. Zhang, *Energies*, 2012, 5, 5190-5197.
34. G. Zhou, L. Li, C. Ma, S. Wang, Y. Shi, N. Koratkar, W. Ren, F. Li and H.-M. Cheng, *Nano Energy*, 2014, 11, 356-365.
35. L. Hu, F. La Mantia, H. Wu, X. Xie, J. McDonough, M. Pasta and Y. Cui, *Advanced Energy Materials*, 2011, 1, 1012-1017.
36. S.-H. Chung and A. Manthiram, *Electrochemistry Communications*, 2014, 38, 91-95.
37. Y.-S. Su, Y. Fu and A. Manthiram, *Physical Chemistry Chemical Physics*, 2012, 14, 14495-14499.
38. S. S. Zhang and D. T. Tran, *Journal of Power Sources*, 2012, 211, 169-172.
39. G. Xu, B. Ding, J. Pan, P. Nie, L. Shen and X. Zhang, *Journal of Materials Chemistry A*, 2014, 2, 12662-12676.
40. G. Pognon, T. Brousse and D. Bélanger, *Carbon*, 2011, 49, 1340-1348.
41. M. Kruk and M. Jaroniec, *Chemistry of Materials*, 2001, 13, 3169-3183.
42. Y.-S. Su and A. Manthiram, *Nature communications*, 2012, 3, 1166-1172.
43. P. G. Bruce, S. A. Freunberger, L. J. Hardwick and J.-M. Tarascon, *Nature materials*, 2012, 11, 19-29.
44. X. Z. Ma, B. Jin, H. Y. Wang, J. Z. Hou, X. B. Zhong, H. H. Wang and P. M. Xin, *Journal of Electroanalytical Chemistry*, 2015, 736, 127-131.
45. C. Barchasz, F. Molton, C. Duboc, J.-C. Leprêtre, S. Patoux and F. Alloin, *Analytical Chemistry*, 2012, 84, 3973-3980.
46. Y. C. Lu, Q. He and H. A. Gasteiger, *J.phys.chem.c*, 2014, 118, 5733-5741.
47. M. J. Lacey, K. EdstrÖm and D. Brandell, *Electrochemistry Communications*, 2014, 46, 91–93.
48. L.-X. Miao, W.-K. Wang, A.-B. Wang, K.-G. Yuan and Y.-S. Yang, *Journal of Materials Chemistry A*, 2013, 1, 11659-11664.
49. J.-Q. Huang, Q. Zhang, S.-M. Zhang, X.-F. Liu, W. Zhu, W.-Z. Qian and F. Wei, *Carbon*, 2013, 58, 99-106.

Figure captions

Fig. 1 Schematic illustration for the preparation process of the PEDOT@S/BP composite.

Fig. 2 N_2 adsorption/desorption isotherm (a) and pore size distribution curve calculated by the BJH methods (The inset calculated by the HK methods) (b) of BP.

Fig. 3 FE-SEM images of BP (a), S/BP (b) and PEDOT@S/BP (c). TEM images of S/BP (d) and PEDOT@S/BP (e). HR-TEM image of PEDOT@S/BP (f).

Fig.4 XRD patterns of PEDOT-PSS, BP, sulfur, S/BP and PEDOT@S/BP.

Fig. 5 Thermogravimetric curves for sulfur, S/BP, and PEDOT@S/BP.

Fig. 6 CV profiles of S/BP-Al cathode (a), S/BP-C cathode (b) and PEDOT@S/BP cathode (c) at a scan rate of 0.1 mV S^{-1}.

Fig. 7 The charge and discharge profiles at the 1st cycle (a), cycle performance (b), rate capability at various rates (c) and Nyquist plots (d) of different cathodes.

Fig. 8 The SEM images of different cathodes before (left) and after (right) 100 cycles (the insert displays the section photographs). S/BP-Al cathode (a, b), S/BP-C cathode (c, d), and PEDOT@S/BP (e, f) cathode.

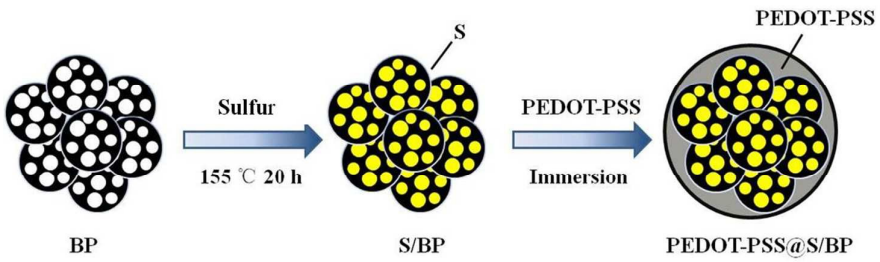

Fig.1 Schematic illustration for the preparation process of the PEDOT@S/BP composite.

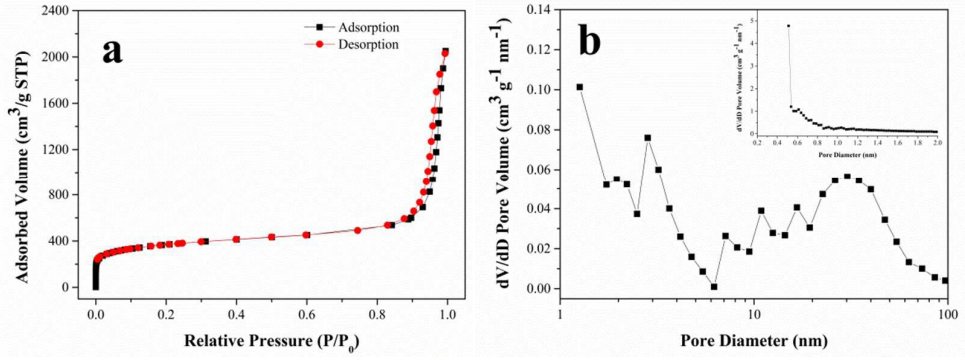

Fig. 2 N_2 adsorption/desorption isotherm (a) and pore size distribution curve calculated by the BJH methods (The inset calculated by the HK methods) (b) of BP.

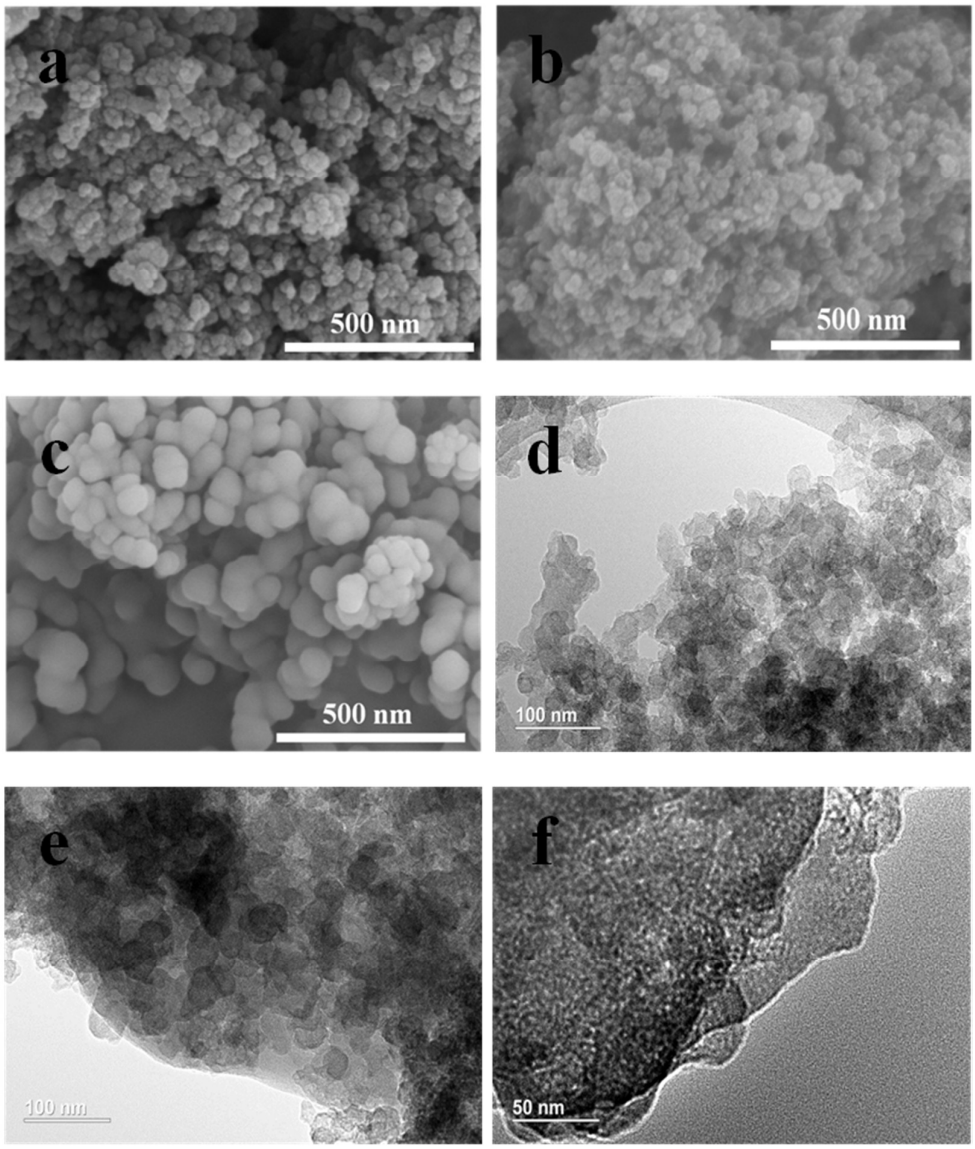

Fig. 3 FE-SEM images of BP (a), S/BP (b) and PEDOT@S/BP (c). TEM images of S/BP (d) and PEDOT@S/BP (e). HR-TEM image of PEDOT@S/BP (f).

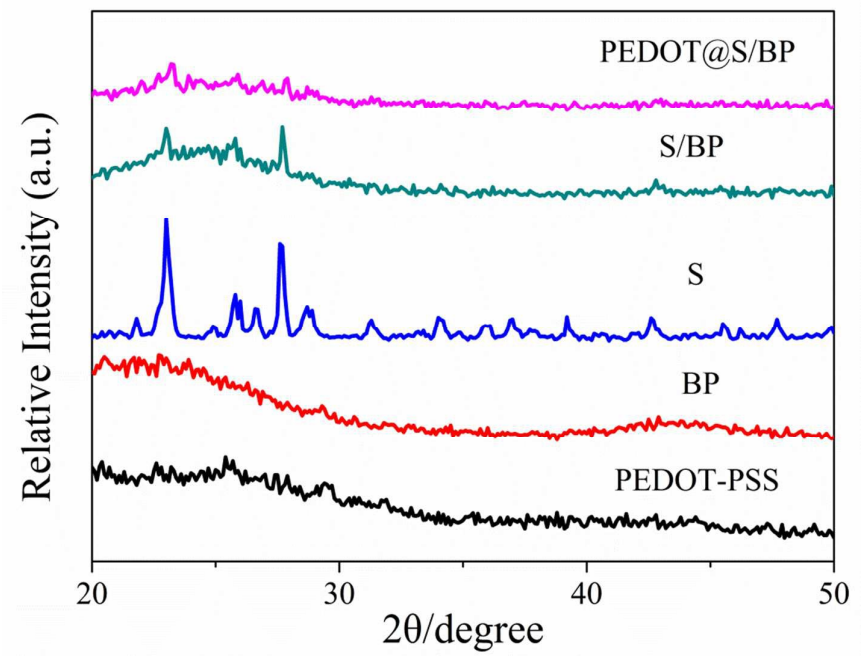

Fig.4 XRD patterns of PEDOT-PSS, BP, sulfur, S/BP and PEDOT@S/BP.

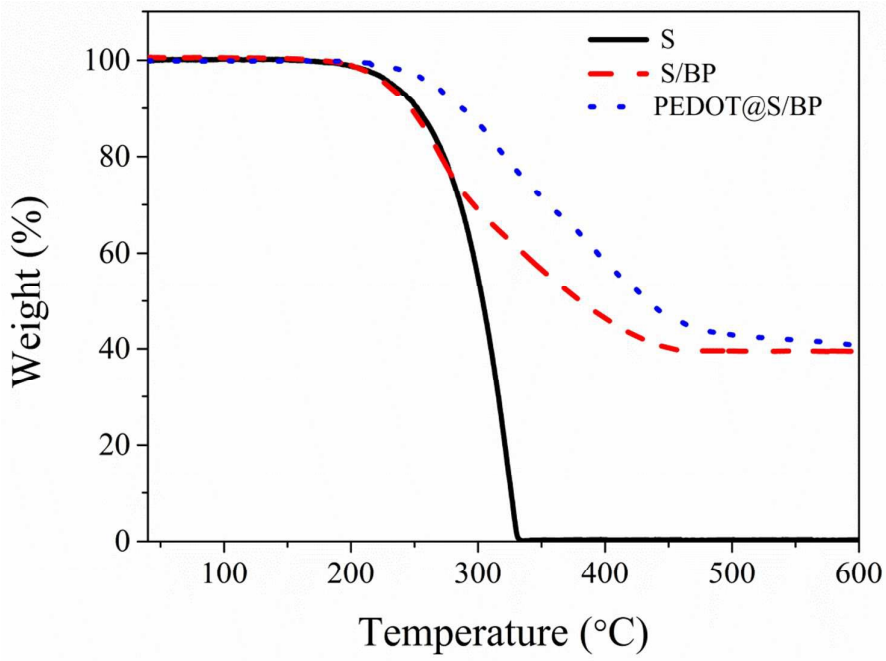

Fig. 5 Thermogravimetric curves for sulfur, S/BP, and PEDOT@S/BP.

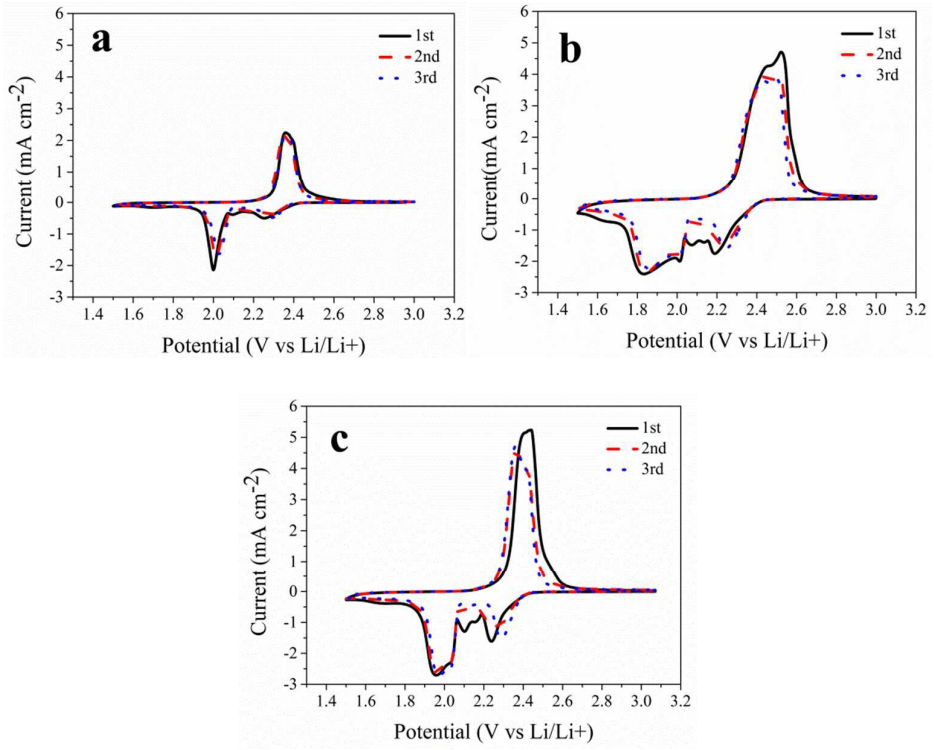

Fig. 6 CV profiles of S/BP-Al cathode (a), S/BP-C cathode (b) and PEDOT@S/BP cathode (c) at a scan rate of 0.1 mV S^{-1}.

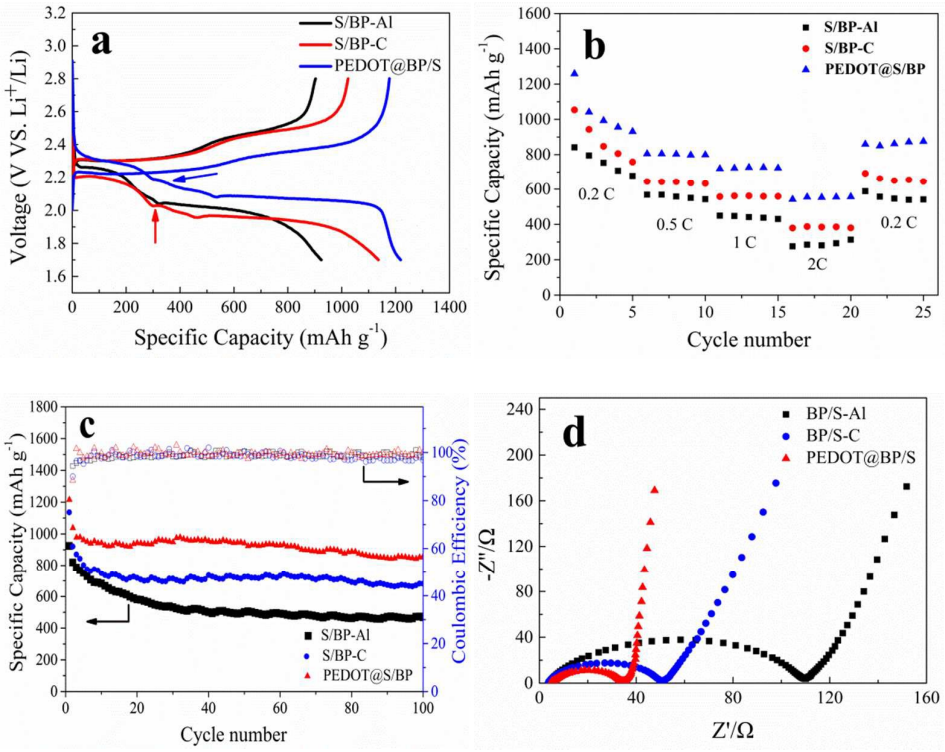

Fig. 7 The charge and discharge profiles at the first cycle (a), cycle performance (b), rate capability at various rates (c) and Nyquist plots (d) of different cathodes.

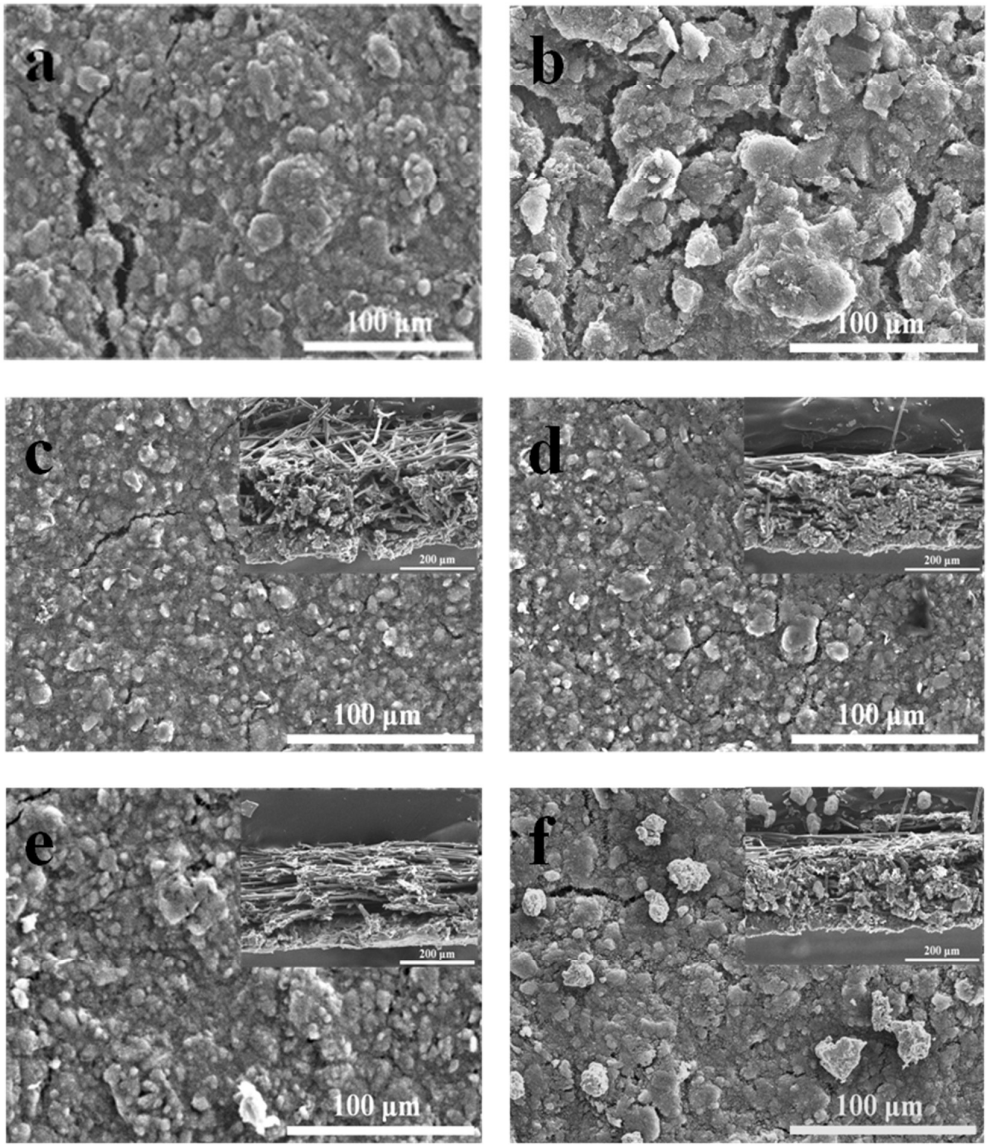

Fig. 8 The SEM images of different cathodes before (left) and after (right) 100 cycles (the insert displays the section photographs). S/BP-Al cathode (a, b), S/BP-C cathode (c, d), and PEDOT@S/BP (e, f) cathode.